Estimating wave energy flux from significant wave height and peak period

Nicolas Guillou

Version of Record: https://www.sciencedirect.com/science/article/pii/S0960148120304560
Manuscript_c754cd5e3ebe14a2c073a0f11a63fb08

Estimating wave energy flux from significant wave height and peak period

Nicolas Guillou[a,*]

[a] *Cerema, Direction Eau Mer et Fleuves, Environnement et Risques, Laboratoire de Génie Côtier et Environnement (LGCE), 155 rue Pierre Bouguer, Technopôle Brest-Iroise, BP 5, 29280, Plouzané, France*

Abstract

Optimum design and location of wave energy converters in the marine environment require accurate assessments of the spatio-temporal variability of the available wave energy flux. However, numerical hindcast databases (commonly exploited for these long-term evaluations) integrate a restricted number of parameters such as the significant wave height H_s or the peak period T_p. Computation of wave power density from hindcast database is thus conducted by relying on simplified formulations derived from approximations of the group velocity and the wave energy spectrum. The present investigation quantified the biases in wave power computation from two standard formulations, based on the energy period and the peak period, respectively. The analysis relied on NOAA observations in 17 locations of the North-West Atlantic, the Gulf of Mexico and the Caribbean Sea. Whereas the energy-period formulation was a very good approximation of the wave power density in deep waters, the peak-period formulation (with a default calibration coef-

*Corresponding author
Email address: nicolas.guillou@cerema.fr (Nicolas Guillou)

ficient $\alpha = 0.9$) overestimated locally, by more than 8%, the available wave energy flux. A refined distribution of α against classes of H_s and T_p was established to reduce these differences, decreasing the relative difference from 9.9% to 0.3% off the Greater Antilles.
Keywords: wave energy converter; wave power; North-West Atlantic; Gulf of Mexico; Caribbean Sea; USA East Coast

---

1. Introduction

The exploitation of the wave resource has raised, over the last decades, significant interest and investment promoting technological developments with a wide range of energy converters tested and deployed in real sea conditions [1]. However, optimum design and location of devices in the marine environment require refined estimations of the available wave power density characterizing, in particular, its evolution on different timescales from monthly to annual periods [2]. These aspects are fundamental as the wave resource may show significant temporal variability liable to impact performances of machines between energetic and low-energetic seasons and years, and thus the computational investment and economical return of a wave energy project [3, 4].

As scarce observations were available in locations of interest, the investigation of wave power variability relied, most of the time, on regional numerical hindcast simulations based on third-generation spectral wave models that provided a continuous and consistent assessment of the wave energy climate on multi-decadal periods of time [2, 5, 6]. However, in many locations, due to limited storage space, the recorded historical and on going sea wave characteristics (at all computational grid nodes) were restricted to integrated wave parameters such as the significant wave height H_s or the statistical periods (peak or mean periods, T_p and T_m) setting aside a detailed assessment of the wave energy spectrum and a computation of the available wave energy flux. This situation was typical of wave hindcast and reanalysis archives primary dedicated to produce statistics and trends of the wave climate in the coastal regions [7, 8]. In these situations, the available resource was es-

timated with simplified formulations that were derived from approximations of (i) the group velocity in deep waters and (ii) the wave energy spectrum based on standard shapes such as Pierson-Moskowitz [9] or JONSWAP [10]. Following these assumptions, the wave energy flux was expressed as a function of the significant wave height and statistical periods, and results were exploited to provide preliminary assessments of the long-term spatial and temporal variabilities of wave power density [11, 12, 13].

Nevertheless, these simplified formulations may present important biases in comparison with the power directly computed from the spectral energy density and the superposition of an infinite number of waves with different heights and frequencies [14, 15]. By exploiting wave observations along the Atlantic coast of the southeastern USA, Defne et al. [14] found that a formulation of wave power based on H_s and T_m overestimated the available wave energy density by 40%. More recently, Ozkan et al. [15] exhibited that a standard equation based on wave height and energy period T_e underestimated the available wave power by an average of 17% in the coastal region of the Florida Peninsula (USA).

Complementing these investigations, the present study estimated and analyzed the differences in wave power computations from simplified formulations by relying on long-term observations of the National Data Buoy Center (NDBC) [16] (National Oceanic and Atmospheric Administration - NOAA) in offshore waters of the North-West Atlantic (off the USA East Coast, the Bahamas, and the Greater and Lesser Antilles), and in the Gulf of Mexico and the Caribbean Sea (Fig. 1, Section 2.1). The investigation considered two standard formulations, widely-used in wave energy resource assessments

and based on the energy period and the peak period, respectively (Section 2.2). Results of these two formulations were compared to a direct computation of the wave power density from the observed spectral energy density (Section 2.3). The analysis was successively dedicated to the estimation of the averaged wave power and the differences at monthly, seasonal and annual time scales (Sections 3.1 and 3.2). A refined distribution of a calibration coefficient against classes of H_s and T_p was finally established to reduce the

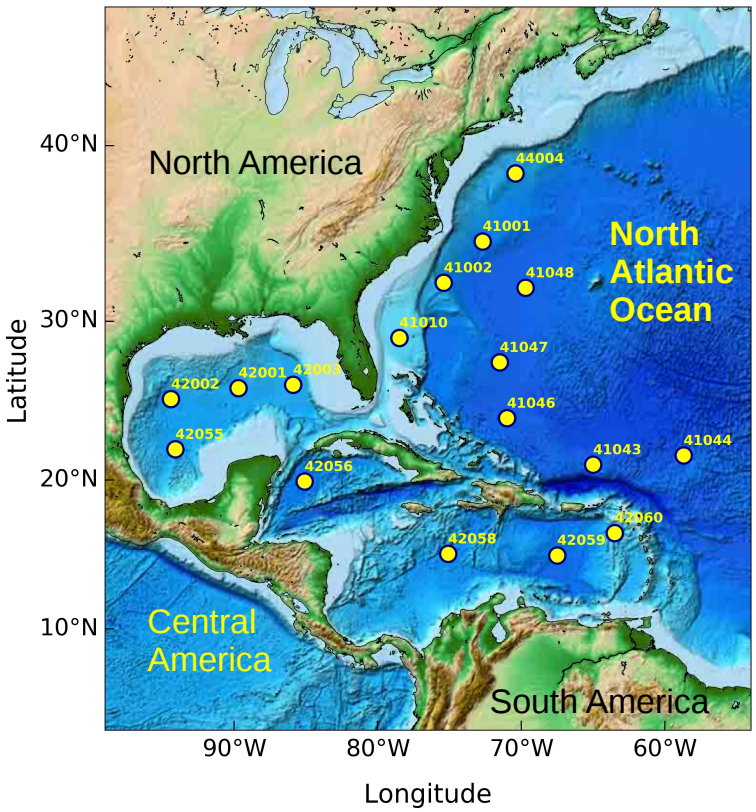

Figure 1: Locations of available wave buoys retained for the evaluation of the wave energy flux.

differences associated with the peak-period formulation (Section 3.3).

2. Materials and methods

2.1. Wave observations

Current study was conducted by exploiting wave energy spectrum measurements, available with a time step of one hour, in NDBC buoys of the North-West Atlantic Ocean [16]. The analysis was restricted to (i) locations with mean water depths over 600 m in order to satisfy the deep water assumption described in Section 2.2, and (ii) observations that cover more than eight years so as to be able to characterize the seasonal and annual variabilities in wave power. This selection resulted in a series of 17 locations disseminated in offshore waters off the USA East Coast, the Bahamas, the Greater and Lesser Antilles, the Caribbean Sea and the Gulf of Mexico (Fig. 1, Table 1).

2.2. Wave power formulations

The available wave energy flux, also denoted the wave power density or wave energy potential (Wm^{-1}, per unit length of wave front) is commonly evaluated as the integral of the product between the group velocity c_g and the spectral energy density E ($\mathrm{m}^2\ \mathrm{s}^{-1}$) with the following relationship

$$P_{spectral} = \rho g \int_0^\infty c_g(f) E(f) df \tag{1}$$

where f is the individual wave frequency, ρ is the density of sea water taken here equal to $\rho = 1025$ kg m^{-3} and g is the gravity acceleration taken equal to $g = 9.81$ m s^{-2}. The group velocity that accounts for the phase speed of

Table 1: Measurement points considered for the evaluation of the available wave energy flux.

Wave	Coordinates		Water depth	Duration
buoys	Lon.	Lat.	(m)	(years)
41001	72.7° W	34.7° N	4479	20
41002	75.4° W	32.3° N	3680	21
41010	78.5° W	29.0° N	895	22
41043	65.0° W	21.0° N	5364	11
41044	58.7° W	21.6° N	5413	9
41046	71.0° W	24.0° N	5523	11
41047	71.5° W	27.5° N	5313	11
41048	69.7° W	32.0° N	5374	11
42001	89.7° W	25.9° N	3208	22
42002	94.4° W	25.2° N	3614	22
42003	85.9° W	26.1° N	3246	22
42055	94.1° W	22.0° N	3580	13
42056	85.1° W	19.9° N	4562	13
42058	75.1° W	15.1° N	4195	12
42059	67.5° W	15.0° N	4863	11
42060	63.5° W	16.5° N	1436	9
44004	70.4° W	38.5° N	3140	13

the envelope of a group of irregular waves is derived from the radian wave frequency $\omega = 2\pi f$ and wave number k as

$$c_g = \frac{\partial \omega}{\partial k} \ . \tag{2}$$

For deep waters ($d/(gT^2) > 10^{-3}$ with d the water depth and T the wave period) and small amplitude waves ($H_s/(gT^2) < 10^{-3}$), the linear wave theory applies resulting in the linear dispersion relationship [17]

$$\omega^2 = gk \tanh(kd) \ . \tag{3}$$

Combining Eqs. 2 and 3, the wave group velocity is expressed as

$$c_g = \frac{\omega}{2k}\left(1 + \frac{2kd}{\sinh(2kd)}\right) \ . \tag{4}$$

In deep waters ($kd >> 1$), the group velocity is approximated as $c_g = g/(2\omega)$ (from expression 4 by including the wave number formulation derived from the linear dispersion equation 3) which results in the following relationship for the available wave energy flux

$$P_1 = \frac{\rho g^2}{4\pi}\int_0^\infty \frac{E(f)}{f} df \ . \tag{5}$$

Eq. 5 is more generally rewritten as a function of the significant wave height $H_s = 4\sqrt{m_0}$ and the wave energy period $T_e = m_{-1}/m_0$ as

$$P_1 = \frac{\rho g^2}{64\pi} H_s^2 T_e \tag{6}$$

with $m_n = \int_0^\infty f^n E(f) df$ the n^{th} order spectral moment. T_e, denoted the wave energy period, represents the period of a single sinusoidal wave that integrates the same amount of energy as in the real sea state.

However, the available hindcast archives are typically limited to bulk parameters that do not include the wave energy period and integrate information on the spectral energy density in a reduced number of points (typically wave buoys). The peak period was thus retained as being more available in

measurements and numerical hindcast databases than other statistical periods such as the spectral mean or zero-upcrossing periods. In this situation, the wave energy period is determined from the available peak wave period by introducing a calibration coefficient α as $T_e = \alpha T_p$, which results in the following formulation of the wave power density

$$P_2 = \frac{\rho g^2}{64\pi} H_s^2 \alpha T_p \ . \tag{7}$$

The calibration coefficient (α) is generally estimated by assuming standard shapes of the wave energy spectrum. It is set to (i) $\alpha = 0.9$ for a standard JONSWAP spectrum with a peak enhancement $\gamma = 3.3$ [11, 12, 13] and (ii) $\alpha = 0.86$ for a Pierson-Moskowitz spectrum [18]. However, further uncertainties exist in relation to the deformation of the wave energy spectrum in coastal seas with values that vary between 0.86 (for wide-band spectra) and 1 (for narrow-band spectra) [11]. Increased differences are furthermore expected in combined sea states including long-crested swell and short-crested wind-sea waves. Indeed, in this situation, the wave spectrum is typically characterized by two energy maxima, in high and low frequencies, and the peak period appears as a rough approximation of the wave energy period. A wide range of α values was thus obtained from the exploitation of real sea states measurements. In a preliminary assessment of the wave energy resource in Cape Verde islands (central Atlantic Ocean), Hagermam [19] considered the wave energy period as being equal to the peak period. In a revised assessment of the wave energy resource around Australia, Hemer et al. [20] estimated this coefficient as $\alpha = 0.857$. By exploiting measurements off Ireland in the Atlantic Marine Energy Test Site, Sheng and Li [21] proposed to retain a coefficient $\alpha = 0.8$ for spectra with two wave energy

peaks. More recently, Ahn et al. [22] analytically derived values of $\alpha = 0.86$ for wind sea and $\alpha = 1.0$ for swell.

The calibration coefficient (α) was furthermore established between T_p and T_e, disregarding the influence of H_s^2 on wave power assessment. This explains why this coefficient may differ from the value that ensures the best fit between the spectral formulation (considered as the reference evaluation) (Eq. 1) and the peak-period formulation (Eq. 7). As classes of H_s and T_p are evolving in relation to sea states conditions, increased temporal variability of α is also expected. Whereas the error associated with this calibration coefficient is less important for wave power computation than the squared error on the significant wave height, refined investigations are finally required to assess the variability of this coefficient against sea wave conditions focusing on its evolution at monthly, seasonal and annual time scales.

2.3. Wave exploitation

The available wave energy flux was successively computed with Eqs. 1, 6 and 7. In all cases, formulations were applied to a finite number of observed spectral energy density components $E_i = E(f_i)$ displayed in n frequencies f_i with $i \in [1, n]$. The initial spectral formulation (Eq. 1) was thus expressed as

$$P_{spectral} = \rho g \sum_{i=1}^{n-1} \frac{1}{2}(c_{g,i}E_i + c_{g,i+1}E_{i+1})(f_{i+1} - f_i) \tag{8}$$

with $c_{g,i} = c_g(f_i)$ the group velocity obtained for frequency f_i with Eq. 4. An iteration process was applied to obtain the wave number from the linear dispersion relationship (Eq. 3). The wave parameters $H_s = 4\sqrt{m_0}$ and $T_e = m_{-1}/m_0$ were computed, in a similar manner, from the evaluation of

spectral moments m_0 and m_{-1} estimated as

$$m_0 = \sum_{i=1}^{n-1} \frac{1}{2}(E_i + E_{i+1})(f_{i+1} - f_i) \tag{9}$$

and

$$m_{-1} = \sum_{i=1}^{n-1} \frac{1}{2}\left(\frac{E_i}{f_i} + \frac{E_{i+1}}{f_{i+1}}\right)(f_{i+1} - f_i) \tag{10}$$

The peak period was finally evaluated from the frequency bin characterizing the wave energy peak. These wave parameters were integrated in Eqs. 6 and 7 to obtain the available wave power densities P_1 and P_2. The peak-period formulation was applied with a default calibration coefficient $\alpha = 0.9$ assuming JONSWAP shape of the wave energy spectrum (Section 2.2). This resulted in three consistent evaluations of the wave power density based on (i) the spectral energy density (Eq. 1), (ii) H_s and T_e (Eq. 6)), and (iii) H_s and T_p (Eq. 7).

3. Results and discussion

3.1. Mean wave power density

Before evaluating the wave power density, computed values of H_s and T_p were compared with the standard meteorological data provided after processing of wave energy spectrum by NDBC [16]. These comparisons confirmed the reliability of the method retained in the present investigation to compute wave parameters from energy spectrum (Section 2.3).

The attention was first dedicated to the estimation of the mean available wave energy flux commonly evaluated in the preliminary stages of a wave energy project (Fig. 2-a). These mean values were computed by averaging the estimations of wave power density during the duration of wave buoys

observations. Whereas these estimations concerned different periods of time, results obtained were consistent with worldwide and local resource assessments [3, 12, 23, 24, 25] exhibiting, with the spectral density formulation 1, values between 15 and 25 $\mathrm{kWm^{-1}}$ in the offshore areas that reduced below 10 $\mathrm{kWm^{-1}}$ in the less exposed regions of the Gulf of Mexico and the Caribbean Sea. A slight increase of wave power density, up to values of 13 $\mathrm{kWm^{-1}}$ was, however, identified in the Carribean Sea (point 42058) in relation to the influence of the Caribbean Low-Level Jet, an easterly zonal wind liable to reach 13 $\mathrm{m\,s^{-1}}$ [25]. These evaluations at measurement points appeared furthermore in the range of values obtained by Defne et al. [14],

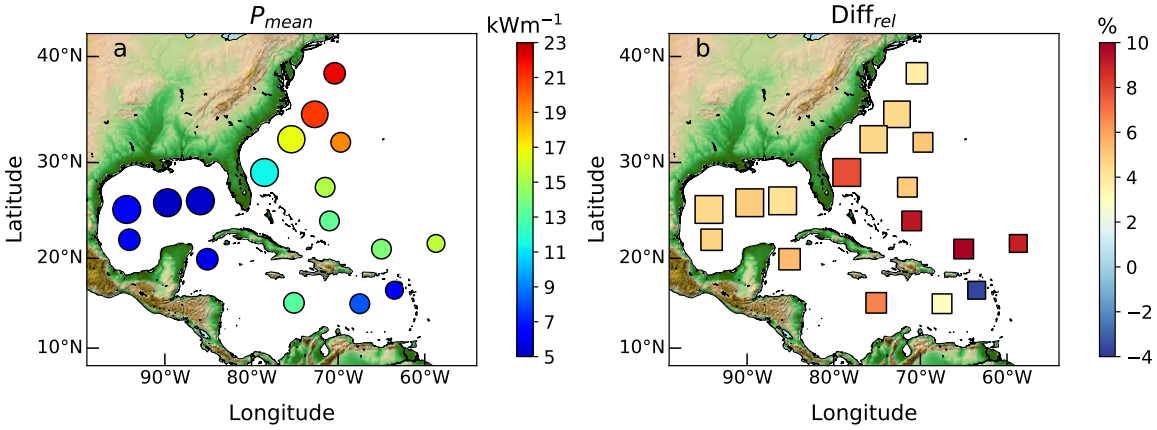

Figure 2: (a) Mean available wave energy flux at measurement points computed with the spectral density formulation 1 and (b) relative differences with respect to the evaluation based on the peak-period (formulation 7) $\mathrm{Diff}_{rel} = 100(\bar{P}_2 - \bar{P}_{spectral})/\bar{P}_{spectral}$ with the overbar denoting the averaged values. Circles diameters were set proportional to the duration of observations. Positive values account for an overestimation of the wave power density with the peak-period formulation 7 while negatives values exhibit an underestimation of the available wave energy flux.

off the USA East Coast, at wave buoys 41001, 41002 and 41010 by applying a moving average filter to wave power observations.

Confirming the approximation of the group velocity in deep waters (Section 2.2), the relationship based on the energy period (Eq. 6) provided nearly the same values of the mean wave power density than the spectral formulation (Eq. 1). As exhibited by scatter plot results of the available wave energy flux at the different time steps (illustration provided at point 41046 in Fig. 3), this energy-period formulation appeared as a very good approximation of the wave energy flux in deep waters promoting the output of T_e in numerical resource assessments. This results contrasted, however, with the investigation conducted by Ozkan and Mayo [15] that exhibited an underestimation of the wave power density by an average of 17% with the energy-period formulation 6 off the Florida Peninsula. Whereas wave buoys considered by Ozkan and Mayo [15] were located in reduced water depths with associated modulation of the group velocity, this tendency was also obtained at point 42003 by more than 3200 m of water depths where the formulation 4 for the group velocity should mathematically converge to $c_g = g/(2\omega)$. As exhibited in the present investigation, reduced differences should thus be obtained in this location between the spectral formulation 1 and the energy-period formulation 6.

The formulation based on the peak period (Eq. 7 with a standard calibration coefficient $\alpha = 0.9$) resulted, however, in increased differences (Fig. 2-b). With an exception at point 42060, this approximation was found to overestimate the mean available wave energy flux at all measurement locations with differences ranging from $3-5\%$ in the Gulf of Mexico and the northern part of USA East Coast to $7-10\%$ off Florida Peninsula, the Bahamas and the

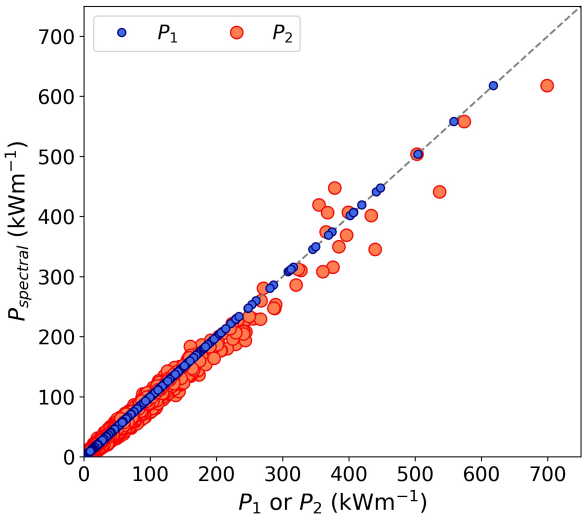

Figure 3: Scatter plot results of $P_{spectral}$ against P_1 and P_2 at wave buoy 41046 (Fig. 1 and Table 1).

Greater Antilles.

3.2. Wave power variability

However, the mean wave power density is a bulk parameter that provides very limited information about the variability of the wave climate and associated uncertainties in power generation, both aspects that are very critical for determining the location of energy converters in the marine environment [2, 4]. For these reasons, differences obtained between wave power formulations were successively exhibited at the annual, seasonal and monthly time scales.

Time series of yearly-averaged available wave energy flux were first computed at measurement points for years that contained more than 95% of observations. Results obtained confirmed the tendency of formulation 7 (with a

calibration coefficient $\alpha = 0.9$) to overestimate the wave power density with differences liable to reach 10% in 2010 at point 41044, off the Lesser Antilles (Fig. 4). These relative differences were averaged at every measurement locations to provide a global estimation of uncertainties associated with the peak-period formulation by adopting the following relationship

$$\mathrm{Diff}_{rel,year} = \frac{1}{n_{year}} \sum_{i=year1}^{year2} 100 \frac{(\bar{P}_{2,i} - \bar{P}_{spectral,i})}{\bar{P}_{spectral,i}} \tag{11}$$

with the overbar denoting the yearly-averaged values and n_{year} the number of years that integrated more than 95% of observations between $year1$ and $year2$. The resulting spatial distribution (Fig. 5) appeared consistent with the analysis conducted on the mean available wave energy flux (Fig. 2) with differences up to 9% off the Greater Antilles.

Time series of monthly-averaged available wave power density were then evaluated at measurement points for years containing more than 95% of data, this in order to gain further insights about the variation of differences at the seasonal time scale (Fig. 6). With an exception at point 42058 characterized by summer energetic conditions associated to the influence of the Caribbean Low-Level Jet [25], a clear contrast was exhibited at measurement locations between (i) winter months with the highest energetic values and (ii) summer months with reduced energy levels. Increased absolute differences (between the peak-period formulation 7 and the spectral formulation 1) were naturally obtained during the most energetic months. However, these differences accounted for nearly the same proportion of the available wave power density during a year (Fig. 7). Whereas a slight increase of these relative differences was exhibited during the winter and spring periods, the spatial distribution retained the same patterns with an averaged overestimation of wave power

density between 8 and 10% in the western part of Florida Peninsula, and off the Bahamas and the Greater Antilles that reduced below 5% in the Gulf of Mexico, the Caribbean Sea and the northern part of USA East Coast.

3.3. Calibration coefficient

3.3.1. Spatio-temporal variations

Whereas the energy-period formulation 6 appeared as a very good approximation of the wave power density in deep waters, the peak-period formulation 7 exhibited further differences. This latter formulation was applied with a standard calibration coefficient $\alpha = 0.9$ by assuming JONSWAP shapes for the wave energy spectrum (Section 2.2). Variations of this coefficient were thus expected with respect to the distribution of wave energy among fre-

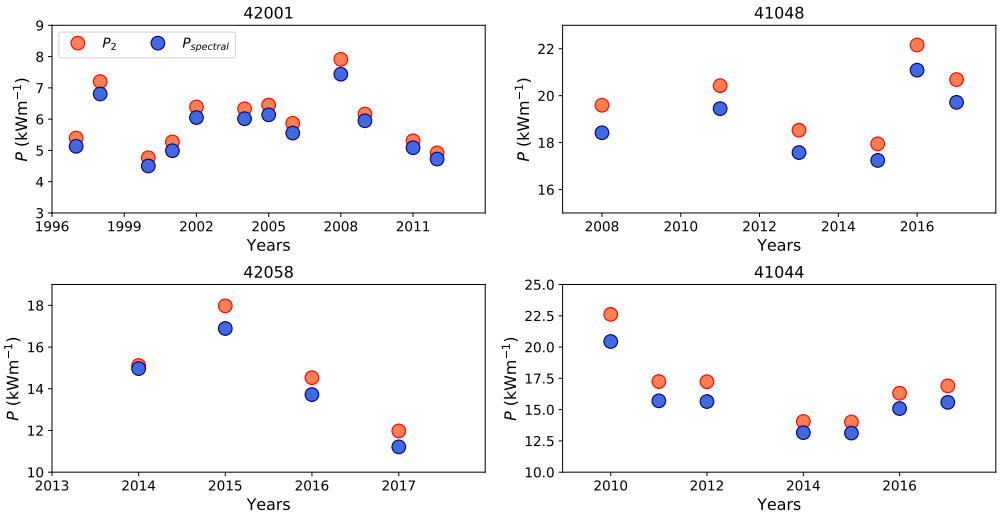

Figure 4: Yearly-averaged available wave energy flux at points 42001, 41048, 42058 and 41044 obtained with the spectral formulation 1 and the peak-period formulation 7 (with a default coefficient $\alpha = 0.9$). The available wave energy flux was computed for years that integrated more than 95% of observations.

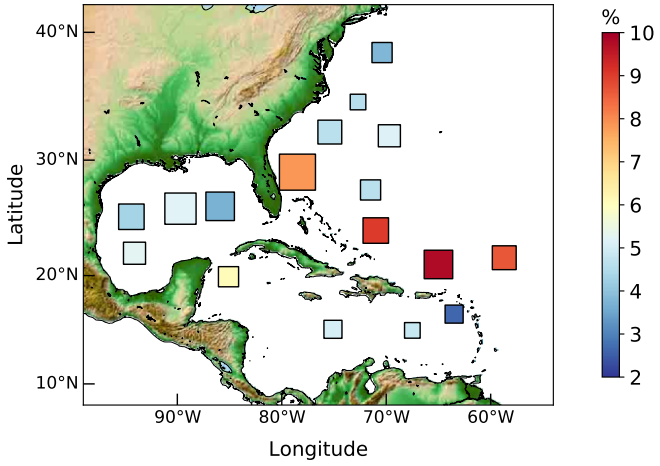

Figure 5: Relative differences, $\text{Diff}_{rel,year}$, in the estimation of yearly-averaged available wave energy flux between the peak-period formulation 7 (with $\alpha = 0.9$) and the spectral formulation 1. The computation was performed for years that contained more than 95% of observations.

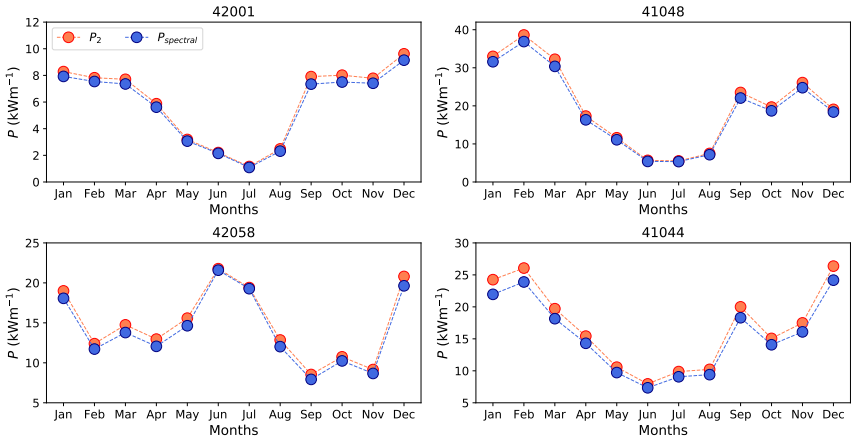

Figure 6: Monthly-averaged available wave energy flux at points 42001, 41048, 42058 and 41044 obtained with the spectral formulation 1 and the formulation 7 based on the peak period. Data were computed for years that integrated more than 95% of observations.

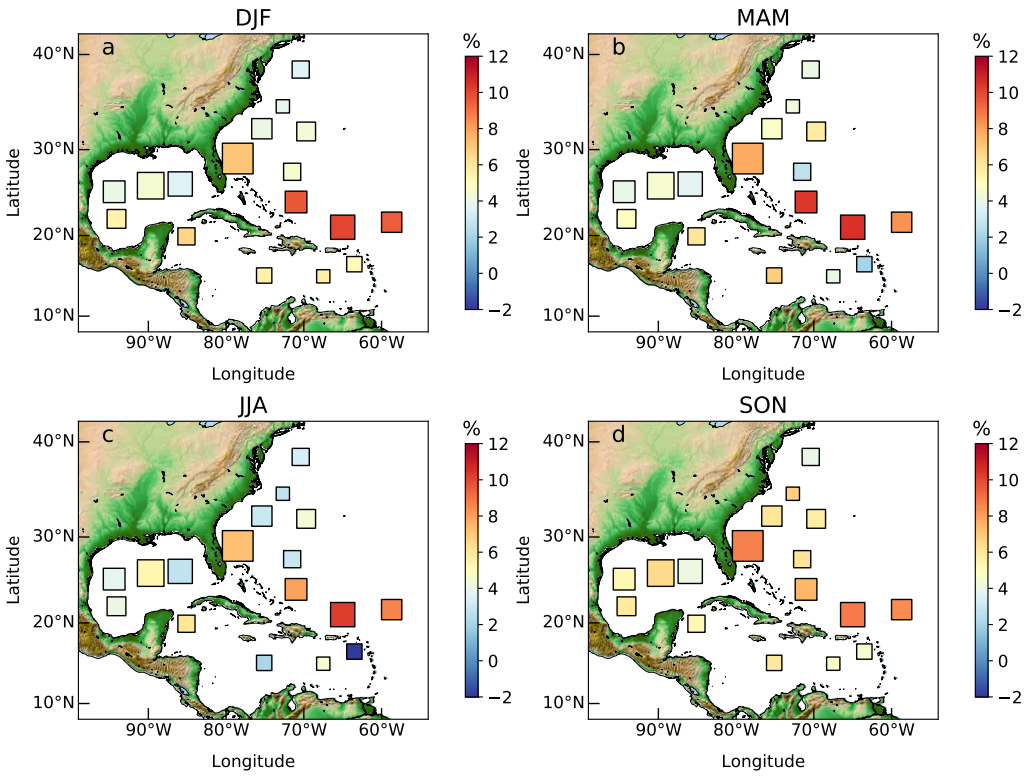

Figure 7: Relative seasonal differences in the estimation of the averaged available wave energy flux between the peak-period formulation 7 and the spectral formulation 1. The four seasons were defined with respect to three-month seasonal time scale as (a) winter (December, January and February), (b) spring (March, April and May), (c) summer (June, July and August) and (d) autumn (September, October and November). The computation was performed for years that contained more than 95% of observations.

quencies, especially in conditions of combined long-crested swell and locally generated wind sea. As P_1 was nearly equal to $P_{spectral}$, α that was defined as the ratio between T_e and T_p (Section 2.2) could also be interpreted as the ratio between $P_{spectral}$ and $P_2 = \rho g^2/(64\pi)H_s^2 T_p$ in deep waters. The calibration coefficient was thus directly analyzed with respect to the computations of available wave energy flux.

However, it was very difficult to retain, at all measurement locations, a constant coefficient that optimized the estimation of the wave power density with the peak-period formulation 7. Adjusting α to provide the best estimate of the mean available wave energy flux (initially displayed in Fig. 2) provided thus values varying between 0.82 and 0.93 (Fig. 8). Lowest values ($\alpha < 0.84$) were obtained in areas (off Florida Peninsula, the Bahamas, the Greater

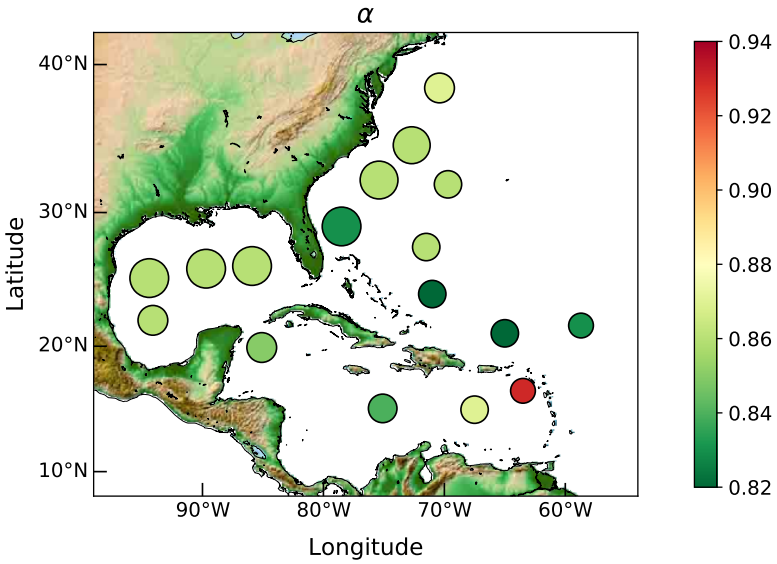

Figure 8: Calibration coefficient that provided the best evaluation of the mean available wave energy flux with the peak-period formulation 7.

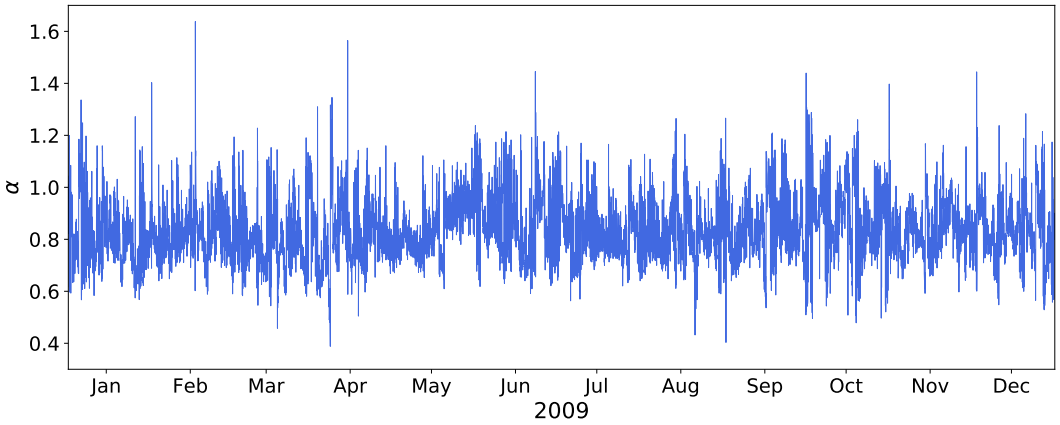

Figure 9: Time series of the calibration coefficient α at point 41046 in 2009.

Antilles and USA East Coast) initially characterized by the more important overestimation of the wave power density while the highest value (up to 0.93) was computed at point 42060 that exhibited an underestimation of the available power. In a given location, α was furthermore characterized by significant variations (between 0.4 and 1.7 at wave buoy 41046, Fig. 9), well beyond the range of values previously identified.

3.3.2. Distribution against H_s and T_p

Nevertheless, as exhibited at wave buoy 41046 (Fig. 10), the calibration coefficient was found to follow tendencies with respect to the significant wave height H_s and the peak period T_p. α was thus found to converge for the most energetic sea states whereas more dispersion was obtained in reduced energy levels with calibration coefficients decreasing as the peak period was increasing. This dispersion of α in reduced-energetic sea states was attributed to two types of wave conditions, (i) dominated by swell (Fig. 11-a) and (ii) resulted from the combination of swell and locally generated wind sea

(Fig. 11-b). In the first type (Fig. 11-a), swell dominated the wave energy spectrum and the peak period was higher than the energy period ($T_p = 11.4$ s / $T_e = 6.5$ s in the illustration) which resulted in reduced values of the calibration coefficient ($\alpha = 0.57$). In the second type (Fig. 11-b), the energy of locally-generated wind seas competed with or dominated the swell energy, and the peak period was reduced ($T_p = 5.9$ s) which increased the calibration coefficient ($\alpha = 1.27$). This tendency was identified at the 17 measurement locations and exhibited with the distribution of averaged values of α in classes of H_s and T_p at the four points 42001, 41048, 42058 and 41044 located in the Gulf of Mexico, the Caribbean Sea, and the oceanic regions off the USA East Coast, the Bahamas and the Antilles (Fig. 12). Whereas the calibration coefficient of a given H_s/T_p class varied between these four locations, it exhibited overall similar distributions against significant wave

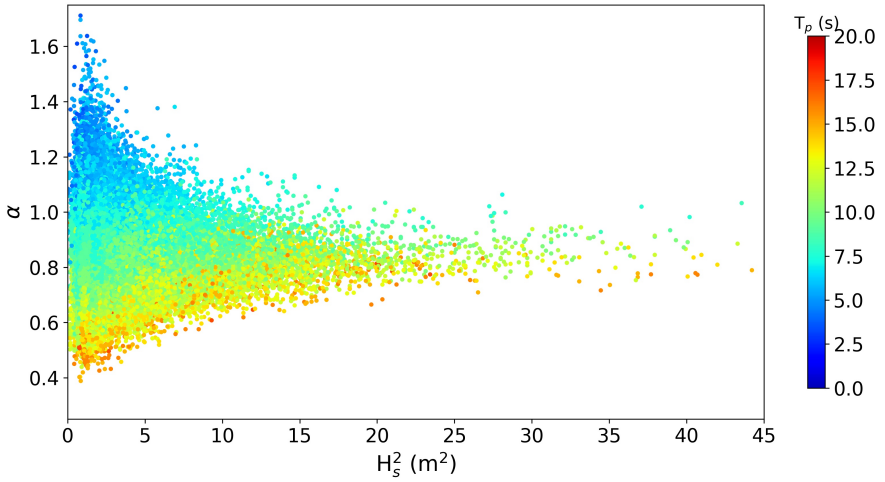

Figure 10: Evolution of the calibration coefficient α with respect to the significant wave height squared and the peak period at point 41046.

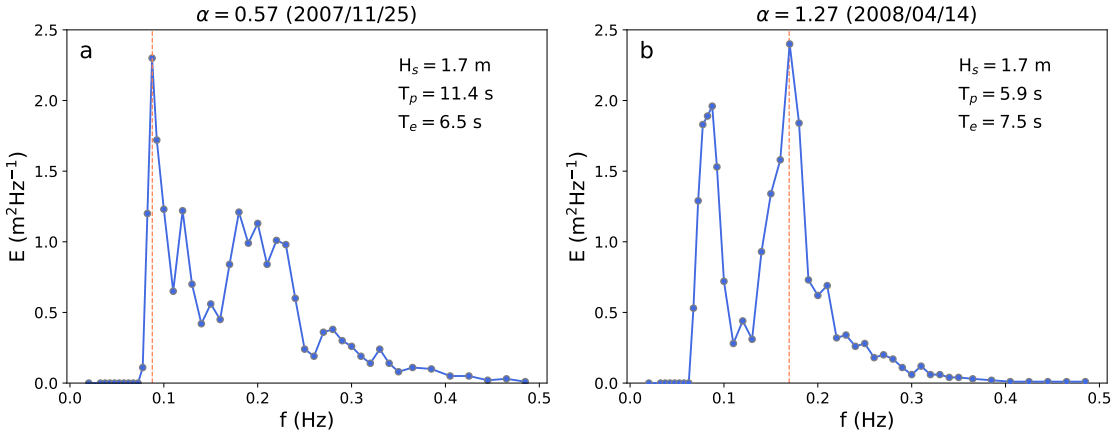

Figure 11: Spectral energy density E with respect to the frequency at point 41046 for conditions of (a) $\alpha = 0.57$ and (b) $\alpha = 1.27$. The vertical line shows the peak frequency.

height and peak period. α was thus found to (i) converge to values between 0.8 and 0.9 for the most energetic sea states, (ii) increase to values over 1.1 in reduced energetic conditions dominated by locally-generated wind seas and (iii) decrease to values below 0.6 in low energetic swell conditions. The distribution of calibration coefficients in low energetic conditions contrasted, however, with the values computed by Ahn et al. [22] ($\alpha = 0.86$ for wind sea against $\alpha = 1.0$ for swell). These differences may be attributed to the shape of the energy spectrum retained by Ahn et al. [22] to derive these coefficients (based on Pierson-Moskowitz spectrum for wind sea and Gaussian spectrum for swell) with single energy peak, only.

On the basis of the distributions of calibration coefficients, a simplified method was proposed to reduce the biases associated with the peak-period formulation 7. Matrices of calibration coefficients computed at the 17 measurement locations were first agglomerated in a single matrice that encom-

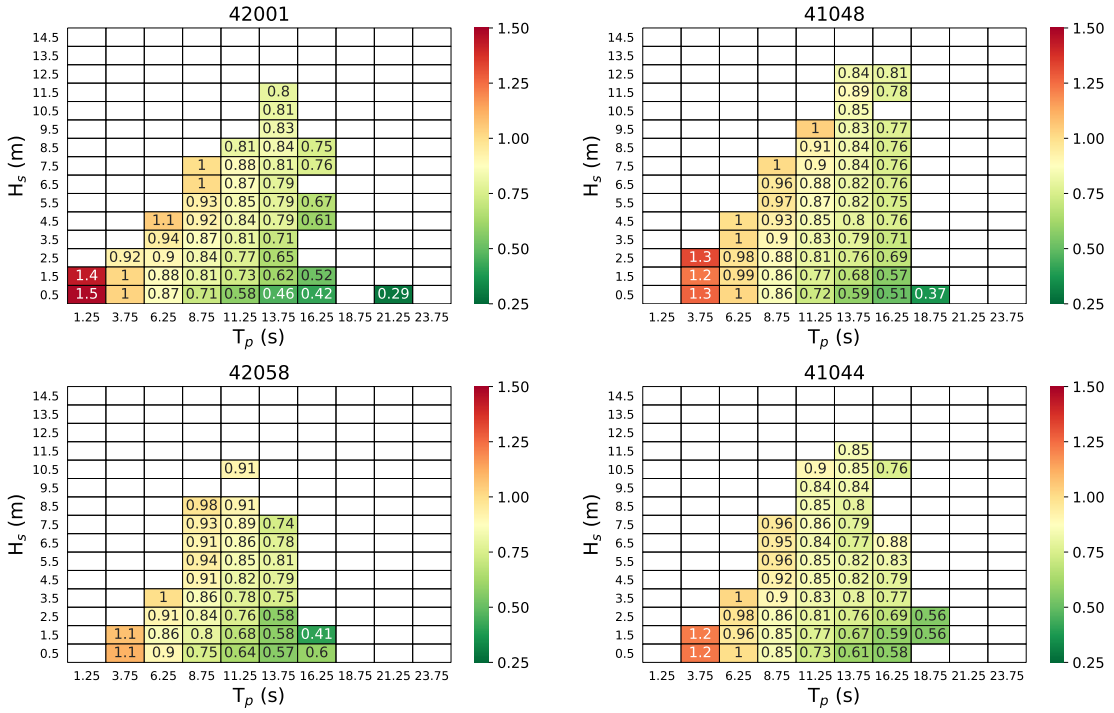

Figure 12: Distribution of the calibration coefficient α in classes of H_s and T_p at wave buoys 42001, 41048, 42058 and 41044.

passed the overall distribution of α against H_s and T_p (Fig. 13). The peak-period formulation was then applied by evaluating the calibration coefficient α with this matrice based on values of H_s and T_p, only. This original computational method (restricted to the knowledge of a single distribution of α coefficients) improved the estimation of the available wave energy flux at the measurement locations. Scatter plots results of $P_{spectral}$ against P_2 (based on T_p) illustrated these improved estimations, particularly noticeable in the highest energetic sea states (Fig. 14). With an exception at point 42060 located in the vicinity of the Lesser Antilles, the new method resulted fur-

thermore in better evaluations of the mean available wave power density (Fig. 15-a). The improvement was particularly noticeable in oceanic wave buoys off the USA East Coast, the Bahamas and the Antilles. The relative difference was thus decreasing from 9.9% to 0.3% at point 41043 off the Greater Antilles. In spite of increased differences at points 41047, 42055 and 42059 in spring and summer, the new method improved finally the estimations of temporal variations of wave power at annual and seasonal time scales (Figs. 15-b and 16).

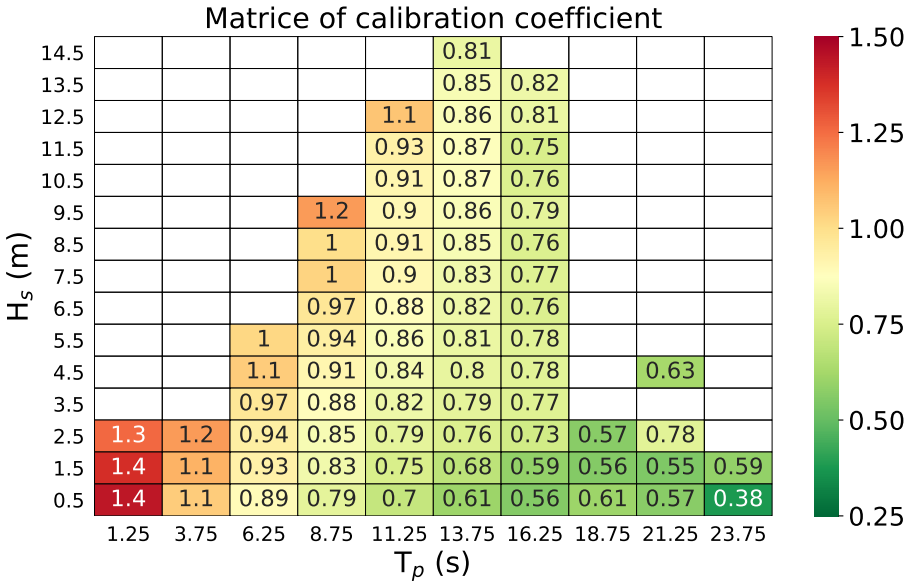

Figure 13: Distribution of the calibration coefficient α in classes of H_s and T_p resulting from the integration of all observations at the 17 wave buoys.

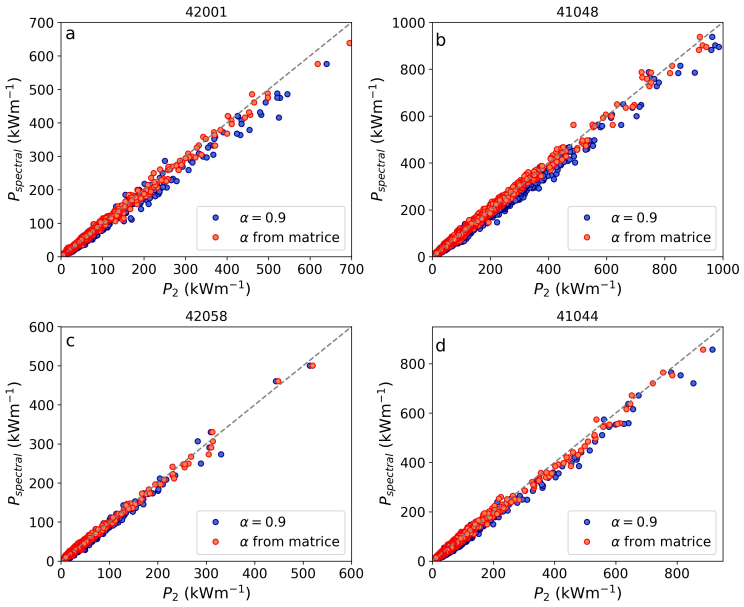

Figure 14: Scatter plot results of $P_{spectral}$ against P_2 with (i) the default calibration coefficient $\alpha = 0.9$ and (ii) the calibration coefficient matrice displayed in Fig. 13 at wave buoys 42001, 41048, 42058 and 41044.

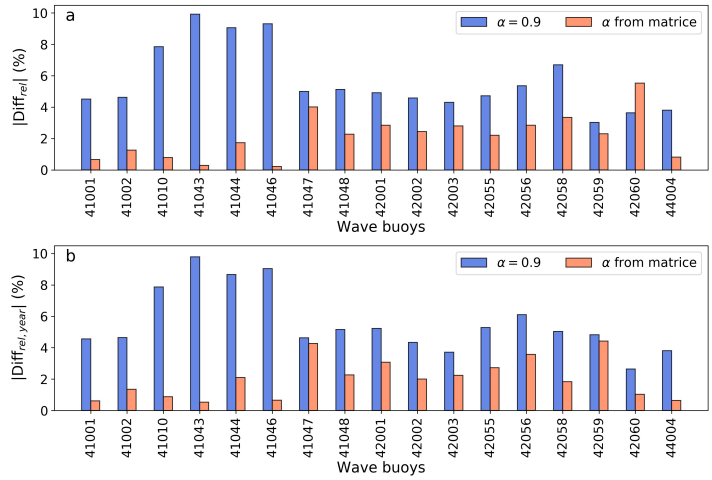

Figure 15: Comparison of the absolute values of the relative differences (a) $|\text{Diff}_{rel}|$ (Fig. 2) and (b) $|\text{Diff}_{rel,year}|$ (Fig. 5) in measurement locations with the peak-period formulation based on (i) the default calibration coefficient $\alpha = 0.9$ and (ii) the calibration coefficient matrice displayed in Fig. 13.

4. Conclusion

Long-term observations of wave conditions were exploited in 17 wave buoys located in mean water depths over 600 m in the North-West Atlantic, the Gulf of Mexico and the Caribbean Sea to assess differences associated with simplified formulations of the available wave energy flux based on the energy period and the peak period. The main outcomes of the present study are as follows:

1. The energy-period formulation 6 based on the approximation of the group velocity in deep waters provided a very good evaluation of the available wave power density and promoted the output of the energy period in numerical hindcast evaluations of wave conditions.

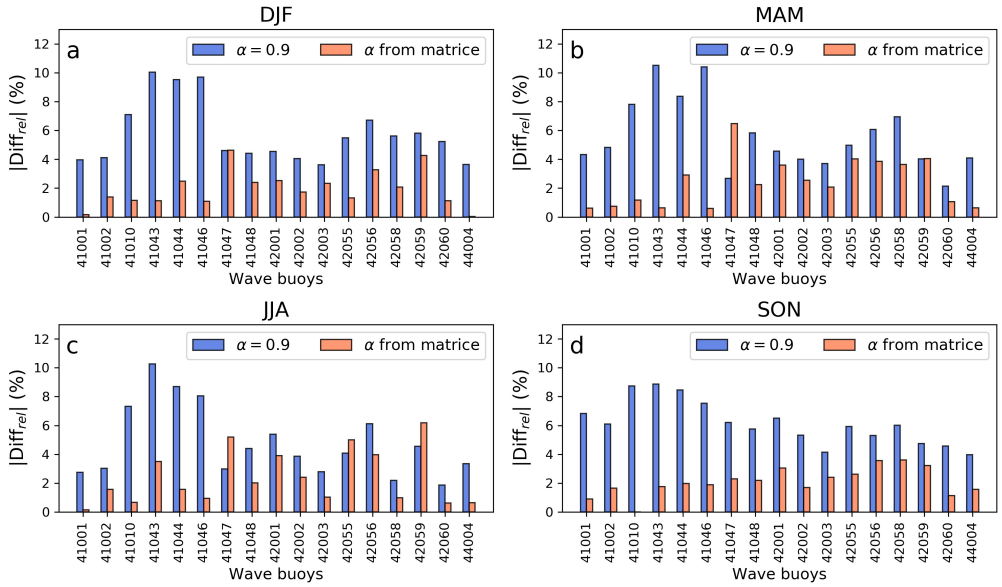

Figure 16: Comparison of the absolute values of the relative differences in the estimation of the averaged available wave energy flux in (a) winter, (b) spring, (c) summer and (d) autumn with the peak-period formulation based on (i) the default calibration coefficient $\alpha = 0.9$ and (ii) the calibration coefficient matrice displayed in Fig. 13.

2. The peak-period formulation 7 parameterized with a default calibration coefficient $\alpha = 0.9$ (matching JONSWAP shape of the wave energy spectrum) exhibited increased differences with a tendency to overestimate the available wave energy flux by more than 8% off Florida Peninsula, the Bahamas and the Greater Antilles.

3. The calibration coefficient was characterized by important spatial and temporal variations. Optimizing this coefficient to provide the best evaluation of the mean available wave power density resulted in values varying between 0.82 and 0.93. This coefficient exhibited furthermore increased variations between 0.4 and 1.7 when focusing on its temporal

evolution at a given location.

4. The calibration coefficient followed, however, tendencies with respect to classes of significant wave height and peak period. While α was found to converge to values around 0.8 and 0.9 for the most energetic sea states, increased dispersion was obtained in reduced energetic conditions. For these reduced energetic levels, α decreased thus to values below 0.6 in swell-dominated conditions and reached values over 1.1 in combined swell and locally-generated wind sea.

5. A refined distribution of α against classes of H_s and T_p was finally established by agglomerating the long-term observations of wave conditions in measurement locations. This single matrice was integrated in the simplified formulation of the available wave power density based on the peak period. Significant improvements were reached for the evaluation of the averaged values at annual, seasonal and monthly time scales.

Further investigations are naturally required to refine the estimation of the distribution of α against classes of H_s and T_p, and assess the robustness of this original method. However, results obtained suggested to rely on varying calibration coefficients to improve the evaluations of the available wave energy flux by exploiting available hindcast predictions and/or observations of H_s and T_p. This method may thus be tested in different oceanic conditions such as the USA West Coast where a series of observations is made available by the National Data Buoy Center. It would furthermore be interesting to analyze the application of this technique in nearshore water depths characterized by different assumptions of the group velocity and reliability of the approach

based on the energy period.

Acknowledgements

In-situ observations were provided by the National Oceanic and Atmospheric Administration (NOAA). The present paper is a contribution to the research program DIADEME ("Design et InterActions des Dispositifs d'extraction d'Energies Marines avec l'Environnement") of the Laboratory of Coastal Engineering and Environment (Cerema, http://www.cerema.fr).

References

[1] A. Falcão, Wave energy utilization: a review of the technologies, Renewable & Sustainable Energy Reviews 14 (2010) 899–918.

[2] S. Neill, M. Hashemi, Wave power variability over the northwest European shelf seas, Applied Energy 106 (2013) 31–46.

[3] J. Portilla, J. Sosa, L. Cavaleri, Wave energy resources: Wave climate and exploitation, Renewable Energy 57 (2013) 594–605.

[4] N. Guillou, G. Chapalain, Annual and seasonal variabilities in the performances of wave energy converters, Energy 165 (2018) 812–823.

[5] N. Guillou, G. Chapalain, Numerical modelling of nearshore wave energy resource in the Sea of Iroise, Renewable Energy 83 (2015) 942–953.

[6] M. Gonçalves, P. Martinho, C. G. Soares, A 33-year hindcast on wave energy assessment in the western French coast, Energy 165 (2018) 790–801.

[7] S. Gallagher, R. Tiron, F. Dias, A long-term nearshore wave hindcast for Ireland: Atlantic and Irish Sea coasts (1979-2012), Ocean Dynamics 64 (2014) 1163–1180.

[8] C. Appendini, A. Torres-Freyermuth, J. López-González, E. T. Mendoza, Wave Climate and Trends for the Gulf of Mexico: A 30-Yr Wave Hindcast, Journal of Climate 27 (4) (2014) 1619–1632.

[9] W. Pierson, L. Moskowitz, A proposed spectral form for fully developed wind seas based on the similarity theory of S.A. Kitaigorodskii, Journal of Geophysical Research 69 (24) (1964) 5181–5190.

[10] K. Hasselmann, T. Barnett, E. Bouws, H. Carlson, D. Cartwright, K. Ende, J. Ewing, H. Gienapp, D. Hasselmann, P. Kruseman, A. Meerburg, P. Muller, D. Olbers, K. Richter, W. Sell, H. Waldden, Measurements of wind-wave growth and swell decay during the JOint North Sea WAve Project (JONSWAP), Dtsch. Hydrogr. Z. Suppl. 12 (A8) (1973) 1–95.

[11] J. Sierra, A. White, C. Mösso, M. Mestres, Assessment of the intra-annual and inter-annual variability of the wave energy resource in the Bay of Biscay (France), Energy 141 (2017) 853–868.

[12] A. Cornett, A global wave energy resource assessment, in: Proceedings of the International Journal of Offshore and Polar Engineering, 2008.

[13] J. Pastor, Y. Liu, Wave Climate Resource Analysis Based on a Revised Gamma Spectrum for Wave Energy Conversion Technology, Sustainability 8 (1321) (2016) –.

[14] Z. Defne, K. A. Haas, H. M. Fritz, Wave power potential along the Atlantic coast of the southeastern USA, Renewable Energy 34 (2009) 2197–2205.

[15] C. Ozkan, T. Mayo, The renewable wave energy resource in coastal regions of the Florida peninsula, Renewable Energy 139 (2019) 530–537.

[16] NDBC, https://www.ndbc.noaa.gov/historical_data.shtml, 2019.

[17] L. Holthuijsen, Waves in Oceanic and Coastal Waters, Cambridge University Press, Cambridge, 2007.

[18] F. Arena, V. Laface, G. Malara, A. Romolo, A. Viviano, V. Fiamma, G. Sannino, A. Carillo, Wave climate analysis for the design of wave energy hervesters in the Mediterranean Sea, Renewable Energy 77 (2015) 125–141.

[19] G. Hagernam, Southern New England Wave Energy Resource Potential, in: Proc. Building 23 Energy'2011, Boston, USA, 2001.

[20] M. Hemer, S. Zieger, T. Durrant, J. O'Grady, R. Hoeke, K. McInnes, U. Rosebrock, A revised assessment of Australia's national wave energy resource, Renewable Energy 114 (2017) 85–107.

[21] W. Sheng, H. Li, A Method for Energy and Resource Assessment of Waves in Finite Water Depths, Energies 10 (460).

[22] S. Ahn, K. A. Haas, V. S. Neary, Wave energy resource classification system for US coastal waters, Renewable and Sustainable Energy Reviews 104 (2019) 54–68.

[23] K. Gunn, C. Stock-Williams, Quantifying the global wave power resource, Renewable Energy 44 (2012) 296–304.

[24] B. Reguero, I. Losada, F. Méndez, A global wave power resource and its seasonal, interannual and long-term variability, Applied Energy 148 (2015) 366–380.

[25] C. Appendini, C. Urbano-Latorre, B. Figueroa, C. Dagua-Paz, A. Torres-Freyermuth, P. Salles, Wave energy potential assessment in the Caribbean Low Level Jet using wave hindcast information, Applied Energy 137 (2015) 375–384.